CHEMISTRY OF MATERIALS

Article

pubs.acs.org/cm

Bandgap-Graded $Cu_2Zn(Sn_{1-x}Ge_x)S_4$ Thin-Film Solar Cells Derived from Metal Chalcogenide Complex Ligand Capped Nanocrystals

Inhyuk Kim,[†] Kyujin Kim,[†] Yunjung Oh,[†] Kyoohee Woo,[‡] Guozhong Cao,[§] Sunho Jeong,*[,⊥] and Jooho Moon*[,†]

[†]Department of Materials Science and Engineering, Yonsei University, 50 Yonsei-ro, Seodaemun-gu, Seoul 120-749, Republic of Korea

[‡]Advanced Manufacturing Systems Research Division, Korea Institute of Machinery and Materials (KIMM), 156 Gajeongbuk-ro, Yuseong-gu, Daejeon 305-343, Republic of Korea

[§]Department of Materials Science and Engineering, University of Washington, 302M Roberts Hall, Box 352120, Seattle, Washington 98195-2120, United States

[⊥]Advanced Materials Division, Korea Research Institute of Chemical Technology (KRICT), 19 Sinseongno, Yuseong-gu, Daejeon 305-600, Republic of Korea

Supporting Information

ABSTRACT: We demonstrate organic residue free, bandgap-graded $Cu_2Zn(Sn_{1-x}Ge_x)S_4$ (CZTGeS) thin-film solar cells based on metal chalcogenide complex (MCC) ligand capped nanocrystals (NCs). The bandgap of the CZTGeS films is tuned by varying the amount of $Sn_2S_6^{4-}$ MCC ligand absorbed on the surface of the Cu_2ZnGeS_4 (CZGeS) NCs, without an undesirable postselenization process. Using CZGeS NCs inks with three different Sn/(Ge+Sn) ratios, bandgap-graded CZTGeS thin films are obtained via multicoating and annealing procedures. Compositional and spectroscopic analyses along the film thickness confirm that the band-graded CZTGeS absorber layer, with a gradually increasing bandgap from the back contact to the *p*−*n* junction, is successfully accomplished. Compared with an ungraded band structured CZTGeS cell, this normal grading structure facilitates both higher short circuit current and open-circuit voltage, facilitating a power conversion efficiency of 6.3%.

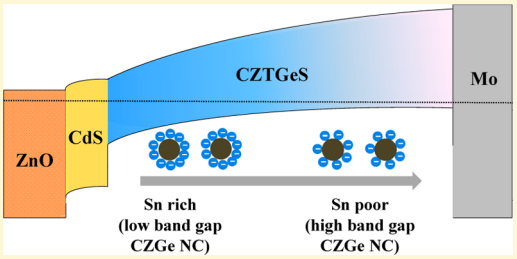

INTRODUCTION

Kesterite, Cu_2ZnSnS_4 (CZTS), has received significant attention as a promising absorber material in thin film-solar cells due to its abundance and nontoxicity as well as desirable optical properties.[1−4] Vacuum-based deposition techniques, generally adopted for device-quality thin films, are unsuitable for large-area, low-cost photovoltaic applications, as they require a large capital investment and a considerable amount of energy. For those reasons, the wet chemistry-based solution route has recently been considered a suitable alternative method for the large-scale and low-cost production of photovoltaic films. In particular, the nanocrystals (NCs)-based ink approach has demonstrated the potential for generating highly efficient CZTS-based thin-film solar cells, which demonstrate high power conversion efficiencies (PCE) of 7.2−9.8%.[5−7] The Agrawal group has reported the high efficiency of 9.8% using Ge-doped CZTSSe nanoparticle inks,[6] and Dupont suggested an approach using a mixture of binary and ternary particles, instead of synthesizing quaternary nanoparticles, achieving a best cell efficiency of 8.5% in nanocrystal-based CZTSSe devices.[7] The selenide compounds have been employed by annealing under Se atmosphere for either tailoring the bandgap in Ge-doped sulfide phases or triggering a vigorous densification reaction through an atomic replacement between S and Se. To achieve the high efficiencies, most precedent researches have performed the postselenization process under the extremely toxic Se atmosphere.[6−11] Taking the toxicity of gaseous Se over the S phase into consideration, it would be highly beneficial to develop a method for fabricating high-efficiency CZTS solar cells without the harmful selenization process, for practical applications. However, to date, the efficiency of pure sulfide CZTS nanocrystal-based devices has only reached a PCE of 3.6%.[12]

One of the characteristic methodologies for improving the conversion efficiency of the CZTS absorber layer is Ge doping into the CZTS phase, which enables the formation of a suitable band alignment between a buffer and an absorber layer, and improves the carrier lifetime as well.[13] However, the large bandgap optical properties in Ge-doped CZTS phases result in a decrease of short circuit current (J_{SC}) at the same time. The J_{SC} can be compensated by introducing a bandgap grading structure;[14] a local bandgap grading approach provides an

Received: April 23, 2014
Revised: May 27, 2014
Published: June 2, 2014

   dx.doi.org/10.1021/cm501568d | Chem. Mater. 2014, 26, 3957−3965

additional electric field in the absorber layers, which reduces the recombination probability, thereby enhancing both the J_{SC} and the open-circuit voltage (V_{OC}).[15] Another way of resolving the shortcomings in CZTS NCs derived solar cells would be to determine how to induce an effective microstructural evolution without the involvement of organic residues that are typically produced by current methods. In general, CZTS NCs are characterized by a high surface-to-volume ratio, which inherently results in severe agglomeration between neighboring particles, as a consequence of intense interparticle physical interactions.[16] Thus, most nanoparticle synthesis involves capping ligands, chemisorbed on the surface of NCs, to provide the repulsive interaction in a liquid phase. Oleylamine (OLA) and trioctylphosphine oxide (TOPO), both of which have long aliphatic carbon chains, have been commonly used as capping molecules, because they offer stable passivation and dispersion stability in nonpolar solvents.[5,9−12] However, these ligands are not easily decomposed and instead leave behind hydrocarbon impurities when annealed under an oxygen-free atmosphere, which has an adverse impact on device performance.[17] To resolve these issues, molecular metal chalcogenide complex (MCC) ligands such as $(SnS_4)^{4-}$, $(Sn_2S_6)^{4-}$, $(Sn_2Se_6)^{4-}$, $(In_2Se_4)^{2-}$, and $(In_2Cu_2Se_4S_3)^{3-}$ have been employed to prevent the NCs from aggregating, by providing electrostatic stabilization via charged surface groups.[18−21] However, the carbon-free absorber layers derived from this chemical approach have shown PCEs below 2%.[21]

Herein, we present for the first time, bandgap tuned, carbon-free solar cells based on Cu_2ZnGeS_4 (CZGeS) NCs capped with $Sn_2S_6^{4-}$ MCC ligands without a selenization process, as presented in Scheme 1 (top panel). The OLA capped CZGeS NCs are ligand-exchanged in a formamide solution containing $(NH_4)_4Sn_2S_6$, by which the OLA ligands are replaced by $Sn_2S_6^{4-}$. The Sn/(Ge+Sn) ratio is controlled by varying the amount of $Sn_2S_6^{4-}$ MCC ligands adsorbed on the surface of the CZGeS NCs, and the bandgap of the absorber layer is graded by the successive coating of CZGeS NCs inks with varying Sn/(Ge+Sn) ratios. From among the various bandgap structures, such as the space charge region (SCR) grading, back surface region (normal) grading, and double grading,[22] we select normal grading, in which the bandgap decreases monotonically toward the $p-n$ junction from a back contact, as depicted in Scheme 1 (bottom panel). The band tunable properties of NCs make it possible to fabricate the carbon residue-free, band-graded CZTGeS films, improving the conversion efficiency up to 6.3%.

EXPERIMENTAL SECTION

CZTGeS and CZGeS Nanoparticle Synthesis. CZGeS nanocrystals were synthesized by a hot-injection method under a N_2 atmosphere. In a typical reaction, 5.1 mmol copper(II) acetylacetonate, 3.6 mmol zinc acetylacetonate hydrate, and 2.1 mmol germanium(IV) chloride were dissolved in 25 mL of oleylamine (70%, OLA), followed by heating to 120 °C under vigorous stirring. As a separate solution, sulfur was dissolved in 17 mL of OLA at room temperature. The solution containing copper, zinc, and germanium was rapidly injected into OLA maintained at 300 °C. After 10 min, the sulfur solution was injected to this OLA precursor solution. After 30 min, the reactor was cooled to room temperature and 10 mL of hexane was added to prevent the aggregation. CZGeS nanoparticles were washed three times using a mixture of hexane:isopropy alcohol = 1:2 volume ratio. The resulting OLA capped CZGeS nanoparticles underwent ligand exchange with a MCC ligand. Typically, 0.1−2.5 M SnS_2 powder was dissolved in 10 mL of ammonium sulfide (40−48% solution in water) to prepare the solution containing $(NH_4)_4Sn_2S_6$ MCC ligands. The 1 g OLA capped particles were redispersed in 4 mL of hexane and mixed with 2 mL of $(NH_4)_4Sn_2S_6$ ligand solution as well as the addition of 4 mL of formamide (Aldrich). The ligand exchange reaction maintained for 12 h under vigorous stirring at room temperature. The resulting MCC capped CZGeS particles were washed using a mixture of acetonitrile:hexane = 1:1 volume ratio. We also synthesized the OLA capped CZTGeS NCs by the same hot-injection method without the ligand exchange, whereas the precursor solution with a different atomic ratio was prepared in which 5.1 mmol copper(II) acetylacetonate, 3.6 mmol zinc acetylacetonate hydrate, 0.84 mmol tin(IV) acetate, and 1.26 mmol germanium(IV) chloride were dissolved in 25 mL of oleylamine.

Scheme 1. Schematic of the Ligand-Exchange Process Using Metal Chalcogenide Complex Ligand and Band Diagram Using Back Surface Region Grading Structure[a]

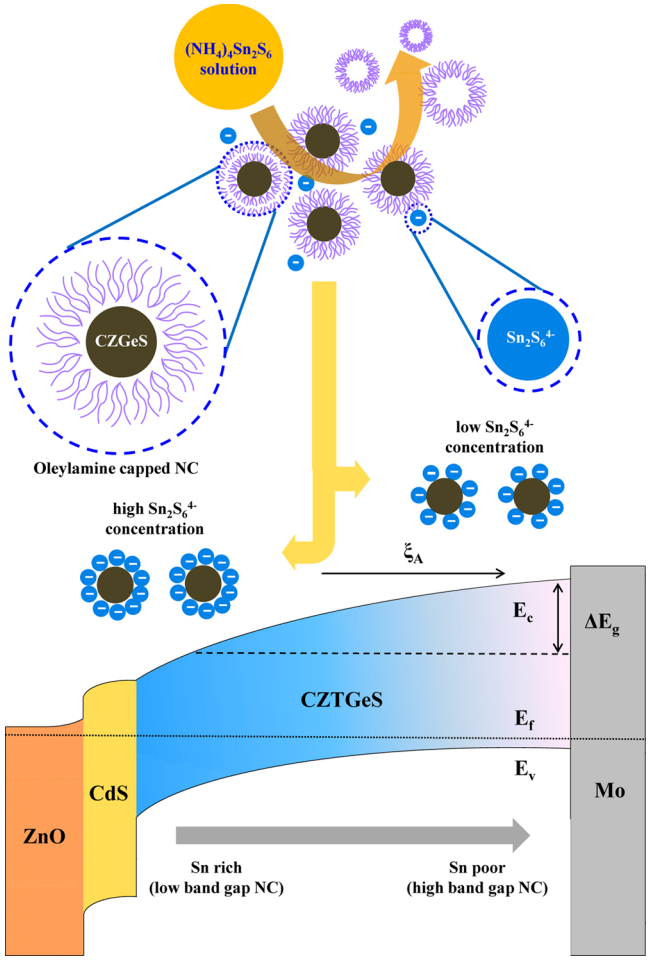

[a]The E_c, E_v, E_f, ΔE_g, and ξ_A are the conduction band energy level, valence band energy level, Fermi energy level, gradient of the band gap, and additional electrical fields, respectively.

Thin-Film Solar Cell Fabrication. To prepare the MCC capped CZGeS nanoparticle dispersion (i.e., ink) for coating, the nanoparticles was dispersed in dimethylformamide at the solid loading of 25 wt %. The OLA capped CZTGeS nanoparticles were also suspended in 1,2-dichlorobenzene at the same solid loading. These inks were milled by a planetary milling machine for 180 min. The formulated ink was coated on molybdenum deposited soda lime glass substrates by a spin-coating method. We fabricated two types of the CZTGeS absorber layers characterized by ungraded bandgap and bandgap-graded structures. To make the ungraded bandgap absorber, the CZGeS nanoparticles ligand-exchanged at a concentration of 2.5 M was deposited by spin coating three times. To understand the influence of the ligand type on

dx.doi.org/10.1021/cm501568d | Chem. Mater. 2014, 26, 3957−3965

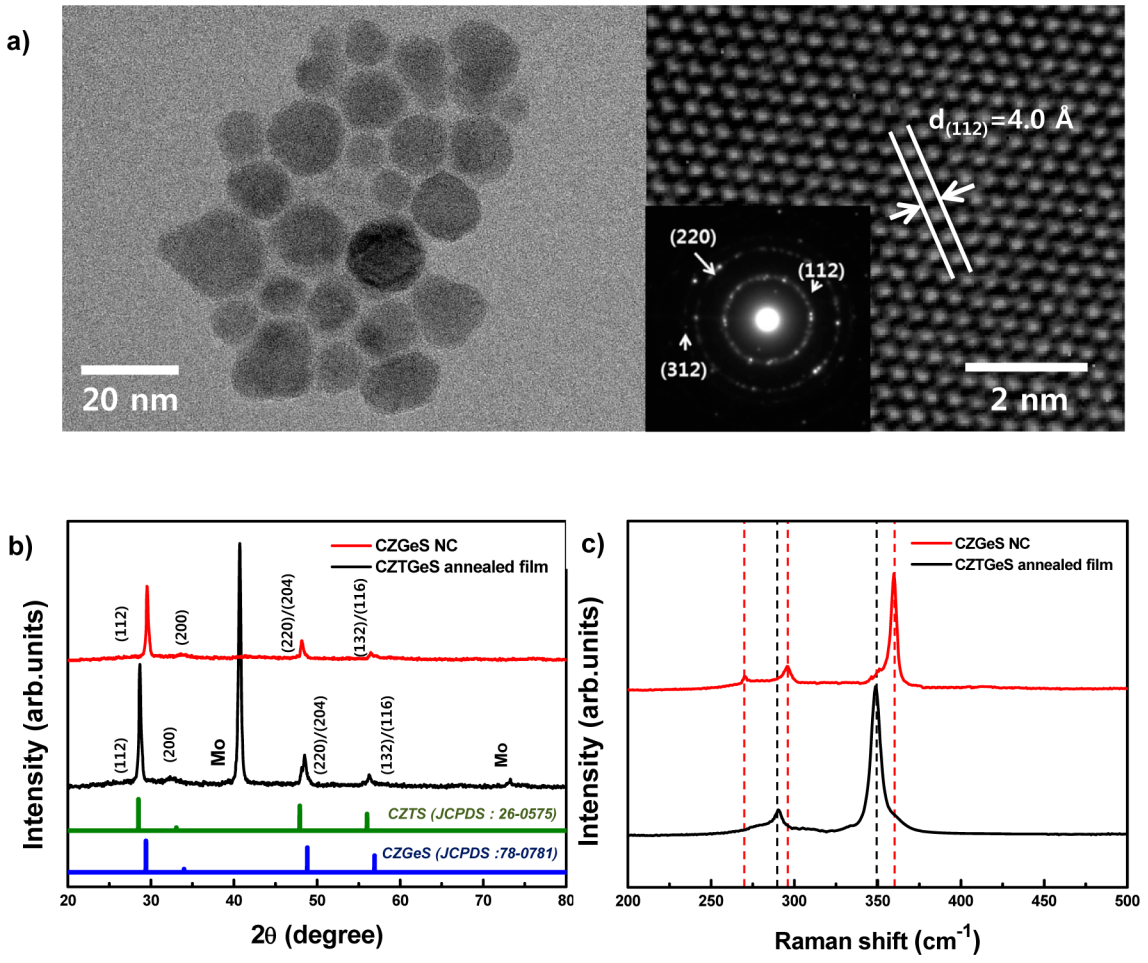

Figure 1. (a) High resolution transmission electron microscopy (HR-TEM) images of the MCC capped CZGeS nanocrystals. The magnified image clearly reveals the lattice distance of the CZGeS. The selected area electron diffraction (SAED) patterns also support the presence of crystalline CZGeS. (b) X-ray diffraction (XRD) patterns of CZGeS nanocrystals on soda lime glass and the CZTGeS film annealed under Ar+H_2S (4%) at 530 °C for 30 min on Mo substrate. (c) Raman spectra of CZGeS nanocystals and the annealed CZTGeS film.

the device performance, the OLA capped CZTGeS NCs were also deposited to form the ungraded absorber layer. To construct the bandgap-graded absorber, on the other hand, three different inks were separately prepared by dispersing the CZGeS nanoparticles ligand-exchanged at a concentration of either 0.2, 1, or 2.5 M. The absorber layer was deposited by a successive coating of the CZGeS nanoparticle inks with increasing MCC content. The resulting thin films were annealed at 530 °C for 30 min under an Ar+H_2S (4%) atmosphere using a tube furnace. The annealed CZTGeS absorber films were processed into photovoltaic devices following the standard procedures including chemical bath deposition of CdS (~60 nm), DC sputtering of *i*-ZnO (~70 nm), RF sputtering of ITO (~250 nm), and thermal evaporation of a patterned Ni/Al grid as the top electrode.

Characterization of the Thin Film and Solar Cells. The size and shape of the synthesized particles were observed by high resolution field emission scanning electron microscopy (FE-SEM, JSM-6700F, JEOL) and high resolution transmission electron microscopy (HR-TEM, Titan G2 60-300, FEI). The phase and crystal structure of the CZGeS particles were confirmed by X-ray diffraction (Ultima IV, Rigaku) with a scan range of 20°−80°. The phases of the CZTGeS films were investigated in detail by using Raman spectroscopy (Lab Ram ARAMIS, Horriba Jovin Yvon) with a wavelength of 532 nm. Fourier transform infrared spectroscopy (FT-IR, Vertex70, Bruker Optic) confirmed OLA removal from the NCs after ligand exchange, and the thermal behavior of the particles under nitrogen atmosphere was examined by thermogravimetry coupled with differential scanning calorimetry (SDT Q600, TA Instruments). To determine the content of $Sn_2S_6^{4-}$ ligand adsorbed onto the particle surface, Inductively coupled plasma atomic emission spectroscopy (ICP-AES, NexION 300, Perkin Elmer) was used for composition analysis of the Ge/Sn ratio in the nanoparticles. To measure the bandgap of thin films, we use the ligand-exchanged nanoparticle at 0.1−2.5 M MCC concentrations, coating it on soda lime glass. After the 530 °C annealed under an Ar+H_2S (4%) atmosphere, we measured the absorption spectra using an ultraviolet−visible (UV−vis) spectrometer (V-530, Jasco). The depth distributions of C, Ge, and Sn were determined and confirmed by second ion mass spectrometry (SIMS 5, Inotof). We confirm a carbon free layer and the Ge/Sn ratio from the surface to bottom to determine the grading structure. We also determined the valence band and conduction band level of the CZTGeS thin films by using ultraviolet photoelectron spectroscopy and inverse photoelectron spectroscopy (ESCALAB 250Xi, Thermo Scientific) under Ar ion beam etching. The IPES uses the low-energy electron gun under an Ar+I_2 atmosphere and the UPS data is calibrated with respect to He+I photon energy (21.21 eV) to estimate the valence band energy. The current density−voltage (*J*−*V*) characteristics and EQE (external quantum efficiency) of the CZTGeS-based cells were analyzed by a solar simulator (Oriel Sol3A Class AAA, Newport Corporation) and an incident photon conversion efficiency (IPCE) instrument (QEX 10, PV Measurements, Inc.), respectively.

■ RESULTS AND DISCUSSION

We synthesized the CZGeS nanocrystals through a hot-injection method, which involves the injection of a metal

dx.doi.org/10.1021/cm501568d | *Chem. Mater.* 2014, 26, 3957−3965

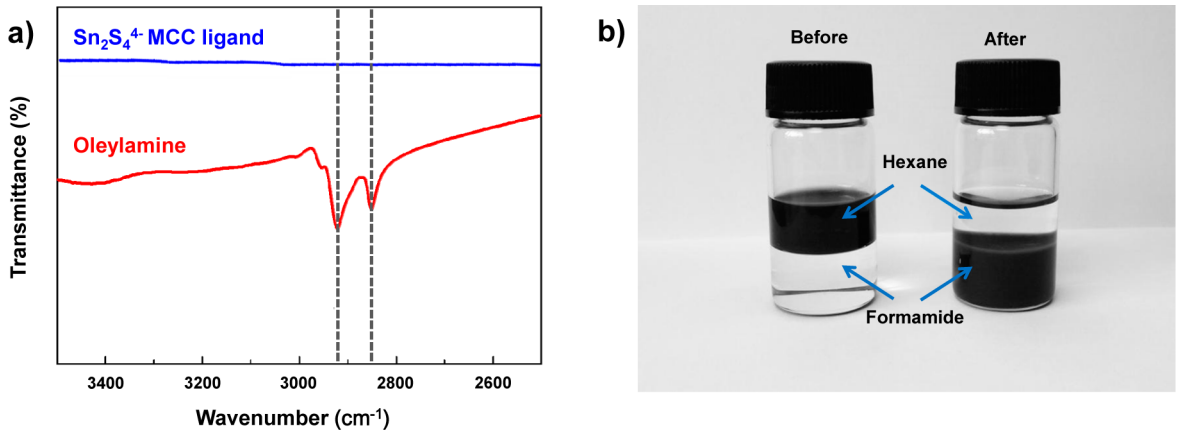

Figure 2. (a) Fourier transform infrared (FT-IR) transmittance spectra for CZGeS nanoparticles capped with oleylamine ligand (red line) and with $Sn_2S_6^{4-}$ MCC ligand (blue line). (b) Picture showing the selective dispersion ability of the particles depending on solvent type. OLA capped particles are dispersed in hexane, but MCC capped particles are well suspended in formamide.

(Cu, Zn, Ge, and S) precursor solution into a hot OLA-containing solution under an inert atmosphere.[15] The atomic ratio of Cu:Zn:Ge:S precursors was 1.7:1.2:0.7:4, which is slightly different from the commonly reported composition (Cu:Zn:Ge:S = 1.7:1.2:1:4). This Cu-poor and Zn-rich composition is known to generate beneficial defect complexes (V_{Cu}+Zn_{Cu}) that can provide a shallow acceptor level so as to lower the Fermi level and subsequently increase the open-circuit voltage. This composition ratio also plays a role in hindering the formation of detrimental defects such as $2Cu_{Zn}$+Sn_{Zn}, which constitute a deep recombination center leading to the loss of V_{OC}. Furthermore, we selected a Ge-deficient composition for the CZGeS NCs so that the Sn atoms in the MCC ligands could readily occupy the Ge vacancy sites during the annealing process. If the Ge site is fully occupied, Sn will likely diffuse into the Cu vacancy; this Sn_{Cu} defect is capable of forming deep levels and increases the conductivity of CZTGeS, in turn, reducing both the shunt resistance and the fill factor (FF).[23] According to high resolution transmission electron microscopy (HR-TEM) images, it was revealed that MCC capped CZGeS NCs have a clean surface morphology without the presence of long carbon chains (Figure 1a). The average particle size was measured to be 16.6 ± 3.3 nm and the magnified view showed a lattice plane spacing of 0.4 nm for the (112) plane. The selected area electron diffraction (SAED) patterns confirmed the formation of phase-pure well-crystallized CZGeS NCs, as determined from the diffractions for (112), (220), and (312) planes. X-ray diffraction (XRD) patterns also revealed that phase-pure CZGeS NCs were synthesized without any secondary phases (Figure 1b). It should be noted that three XRD diffraction peaks at 2θ = 29.3°, 48.8°, and 57.9° overlap with those of copper sulfide (Cu_2S) and zinc sulfide (ZnS), so that the phase purity of CZGeS cannot be confirmed solely by XRD analysis. Therefore, Raman spectroscopy was utilized to obtain further insight into the phase identification (Figure 1c). As-synthesized and ligand exchanged NCs exhibited strong peaks at 360, 291, and 272 cm^{-1}, all of which are assigned to kesterite CZGeS.[24] No additional peaks corresponding to secondary phases such as Cu_2S and ZnS were detected.

To clarify the complete surface exchange between OLA and $Sn_2S_6^{4-}$ ligands, the surface chemical structure was investigated using Fourier transform infrared (FT-IR) spectroscopy. The OLA capped NCs exhibited peaks at 2935 and 2850 cm^{-1}, attributed to C−H asymmetric stretching and symmetric stretching in the OLA molecule, respectively (Figure 2a).[18] These peaks were not observed for MCC ligand capped NCs, which is indicative of the complete removal of OLA. Thermogravimetry coupled with differential scanning calorimetry (TG-DSC) analysis also confirmed the removal of the OLA (Supporting Information, Figure S1a). The OLA capped CZGeS NCs showed the OLA decomposing, with 7% weight loss, at 350 °C accompanying the endothermic peak. On the other hand, for the MCC capped NCs, no weight loss was observable near the 350 °C (Supporting Information, Figure S1b), indicative of the absence of OLA on the surface of MCC capped NCs.[12] This data show that the any OLA was adsorbed on the MCC capped NCs. A dispersion test visually proved the removal of the OLA from the surface of the NCs (Figure 2b). The NCs dispersion property is predominantly dependent on the characteristics of surface molecules. The OLA capped NCs were dispersed only in a nonpolar solvent, hexane, whereas the MCC ligand capped NCs were suspended only in a polar solvent, formamide.

Supplying thermal energy during an annealing process under Ar+H_2S (4%) causes the Sn elements in the $Sn_2S_6^{4-}$ ligand capped CZGeS NCs to diffuse into the crystal lattice of CZGeS, undergoing a phase transformation into $Cu_2ZnSn_{1-x}Ge_xS_4$ (CZTGeS). The phase transformation was confirmed by XRD analysis (Figure 1b). The XRD peaks for an annealed CZTGeS film shifted toward a lower angle, as compared to a ligand exchanged, unannealed CZGeS particulate layer, because the incorporation of Sn with its large atomic radius enlarges the lattice parameter. All diffraction patterns corresponded to kersterite CZTGeS (JCPDS Card No. 78-0781) without the involvement of any secondary phases. Raman analysis also confirmed the formation of phase pure CZTGeS films in the absence of Cu_2S, SnS, and ZnS subphases (Figure 1c).

The amount of $Sn_2S_6^{4-}$ ligand adsorbed on the CZGeS particles was controlled by varying the concentration of $(NH_4)_4Sn_2S_6$ MCC solution in a ligand exchange procedure. To analyze the composition, and Sn/(Ge+Sn) ratio, for annealed $Cu_2ZnSn_{1-x}Ge_xS_4$ (CZTGeS) films, absorber films were prepared using inks containing CZGeS NCs, exchanged with different MCC ligand concentrations. The particulate films were annealed at 530 °C for 30 min under Ar+H_2S (4%), prior to the composition analysis by ICP-AES. Table 1 summarizes the composition of annealed CZTGeS films. The Sn/(Ge+Sn)

dx.doi.org/10.1021/cm501568d | Chem. Mater. 2014, 26, 3957−3965

Table 1. Composition of the Annealed CZTGeS Absorbers Which Is Synthesized under the Varying $Sn_2S_6^{4-}$ Ligand Concentrations As Determined by ICP-AES[a]

MCC concentration [M]	composition molar ratio (Ge+Sn)/Zn	composition molar ratio Sn/(Ge+Sn)	optical bandgap (eV)
0.1 M	0.68	0.04	1.90
0.2 M	0.71	0.11	1.84
0.4 M	0.73	0.21	1.77
1 M	0.79	0.41	1.68
2 M	0.83	0.46	1.66
2.5 M	0.84	0.48	1.64

[a]The optical bandgap for the corresponding films determined by UV−vis spectroscopy is also shown. The films were annealed at 530 °C for 30 min on Mo substrate under Ar+H_2S (4%) atmosphere.

ratio increased from 0.04 to 0.48 by increasing the concentration of $(NH_4)_4Sn_2S_6$ solution from 0.1 to 2.5 M. The lower variation of the Sn/(Ge+Sn) ratio, compared to the variation of the MCC solution concentration, is indicative of some Sn loss during the annealing of the $Sn_2S_6^{4-}$ ligand capped NCs. For the CZGeS nanoparticles treated with 1 M ligand exchange solution, the ICP-AES analysis determined 25.4 at% Sn loss during the annealing (Supporting Information, Table S1). However, it should be noted that this limited Sn/(Ge+Sn) ratio controllability still suggests the possibility of tuning the bandgap of the CZTGeS absorber layers by adjusting the amount of adsorbed MCC ligand. Ford et al. reported that the bandgap of CZTGeS films can vary from 1.5 to 1.95 eV with increasing Ge content, implying that the bandgap of CZTGeS film decreases as the Sn content increases.[15] The conduction band minimum of CZTGeS depends on the antibonding of Sn and Ge orbitals. As Ge is replaced by Sn, Ge−S atom *s*−*s* and *s*−*p* orbital repulsions are weakened, and Sn *s* and anion *p* hybrid orbitals are strengthened in CZTGeS. This results in a decrease in the antibonding conduction band minimum, thereby decreasing the bandgap.[25] To elucidate the band gap tunability and its dependence on the Sn/(Ge+Sn) ratio, we measured the optical bandgap for annealed CZTGeS films using ultraviolet−visible (UV−vis) spectroscopy. The bandgap was determined to be 1.64−1.90 eV by line fitting in a plot of $(\alpha h\nu)^2$ vs $h\nu$ where α, h, and ν are the optical absorption coefficient, Planck's constant, and frequency, respectively (Figure 3 and Table 1). The bandgap decreased with increasing Sn contents in MCC ligand capped CZGeS NCs. The empirical relationship between the bandgap and the Sn/(Ge+Sn) ratio was obtained by a linear regression (Supporting Information, Figure S2); the linear compositional dependence fit relatively well to the previous data by Ford et al.

Utilizing those bandgap tunable properties, we designed a normal grading band structure for high efficiency solar cells.[26] According to a recent simulation study for $Cu(In_{1-x}Ga_x)S_2$ solar cells, excessive space charge region (SCR) grading may cause a strong barrier at a *p*−*n* junction and generate a carrier recombination site.[27] Consequently, we chose the normal grading structure to avoid these problems. To realize the band grading structure, we fabricated the absorber layer by successive coatings of CZGeS NCs inks with varying adsorbed MCC ligand contents. The bottom layer, in contact with a Mo electrode, was prepared from CZGeS NCs exchanged with 0.2 M $(NH_4)_4Sn_2S_6$ solution, which led to the formation of a CZTGeS absorber layer with a bandgap of ∼1.84 eV. This high

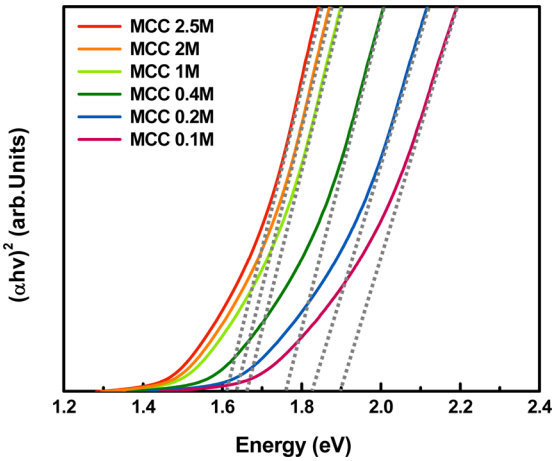

Figure 3. Plot of $(ahv)^2$ as a function of hν for the absorption spectrum of CZTGeS films coated on soda lime glass. The films were annealed at 530 °C under Ar+H_2S (4%) atmosphere. The bandgap energy of the CZTGeS film derived from CZGeS NCs ligand-exchanged at the concentration of 0.1 M $(NH_4)_4Sn_2S_6$ solution (purple) was ∼1.90 eV; ∼1.84 eV for the film from CZGeS NCs ligand-exchanged at 0.2 M (blue); ∼1.77 eV for the film from CZGeS NCs ligand-exchanged at 0.4 M (dark green); ∼1.68 eV for the film from CZGeS NCs ligand-exchanged at 1.0 M (yellow green), ∼1.66 eV for the film from CZGeS NCs ligand-exchanged at 2.0 M (orange); ∼1.64 eV for the film from CZGeS NCs ligand-exchanged at 2.5 M (red).

bandgap bottom layer might decrease the external quantum efficiency due to the transmission loss of long-wavelength light. To facilitate the absorption of long-wavelength light, the middle layer was obtained from CZGeS NCs exchanged with 1 M MCC ligand solution, which likely results in a bandgap of ∼1.68 eV. Finally, we completed the formation of the upper layer using CZGeS NCs treated with 2.5 M ligand solution, leading to the bandgap of ∼1.64 eV. To compare the band grading effect, we also fabricated an ungraded bandgap structure using only NCs treated with 2.5 M solution. The film thickness of the ungraded layer was similar to the one of the bandgap-graded absorber.

The morphologies of the prepared absorber layers were investigated using field emission scanning electron microscopy (FE-SEM). The as-prepared bandgap-graded CZGeS NCs film showed a crack-free microstructure without interlayer delamination (Supporting Information, Figure S3a). The sulfurized CZTGeS absorber also exhibited a relatively dense microstructure, consisting of large grains (1−1.5 μm) without significantly large pores, while having a thickness of ∼1.1 μm (Supporting Information, Figure S3b). Note that the cross sectional image does not show a bilayer microstructure. Such a bilayer structure, composed of an upper polycrystalline large-grain layer and a lower fine-grained layer, is usually observed in organic ligand capped NCs derived absorbers in which carbon impurities are left behind even after vigorous annealing at high temperatures, which hinders the grain growth and in turn results in a fine-grained bottom layer.[25] For comparison, we also produced an OLA capped CZTGeS NCs derived absorber film. The cross sectional image of the resulting layer shows a typical bilayer microstructure (Supporting Information, Figure S3c). To confirm the presence of carbon impurities in the bottom fine-grained layer, energy dispersive X-ray (EDX) elemental line scan analysis was performed (Supporting Information, Figure S4). The compositional mapping analysis

dx.doi.org/10.1021/cm501568d | *Chem. Mater.* 2014, 26, 3957−3965

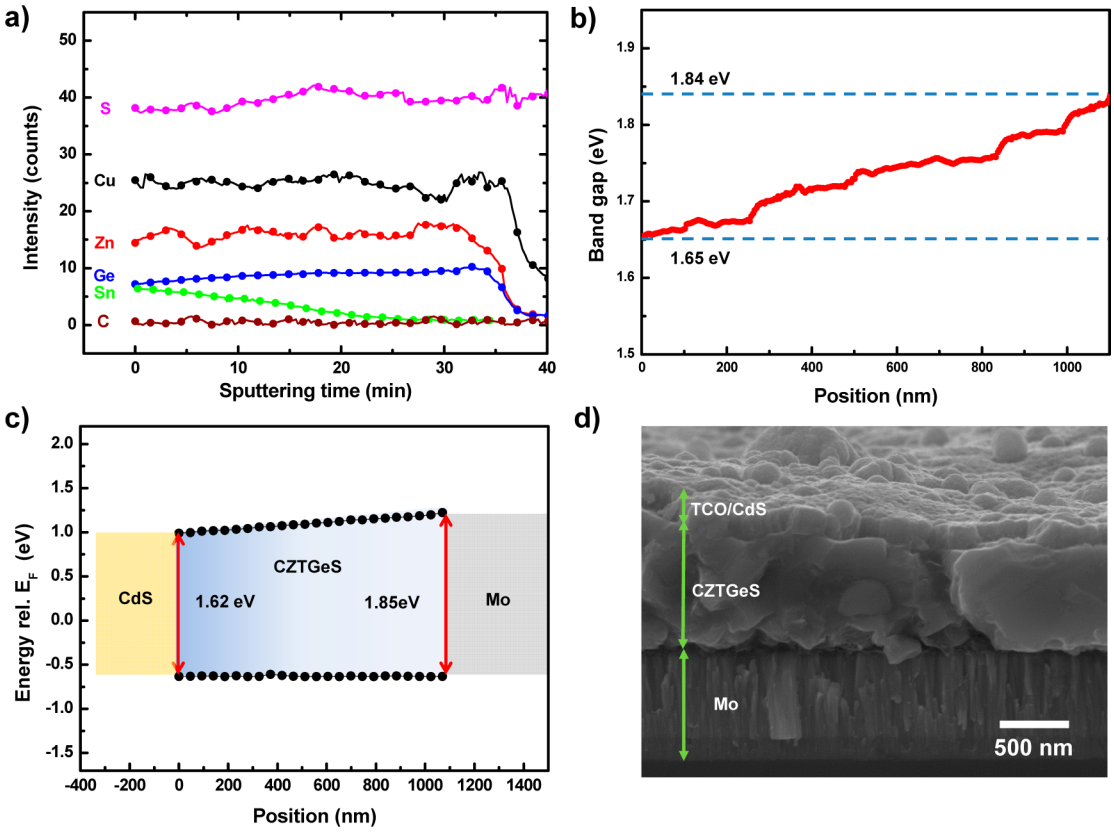

Figure 4. (a) SIMS data of bandgap-graded annealed film to determine the compositional distribution across the film. (b) Sn/(Ge+Sn) ratio across the depth of the bandgap-graded absorber determined by SIMS measurement (Figure 4a) is converted to the optical bandgap using the linear relationship obtained in Figure S2 (Supporting Information). (c) Band alignment of graded CZTGeS film measured by UPS and IPES. We measure the VBM and CBM data as a function of position and conversion it to bandgap. The bandgap values were increased from 1.62 to 1.85 eV. (d) Bandgap-graded CZTGeS-based thin-film solar cell annealed under AR+H_2S (4%) at 530 °C for 30 min. The nanoparticle films were deposited on Mo coated SLG substrate, followed by a successive deposition of CdS, *i*-ZnO, and ITO to complete the device fabrication.

revealed the existence of excess carbon moieties at the bottom of the film. Notably, the MCC ligand capped NCs derived absorber films were free of carbon impurities. For the CZTGeS absorber layer fabricated from ligand exchanged CZGeS NCs, Cu, Zn, Sn, Ge, and S were well distributed throughout the film, while carbon was rarely detected (Supporting Information, Table S2). This fact clearly suggests that CZGeS NCs capped with MCC ligands as a replacement of OLA allows us to form carbon-free, uniformly dense CZTGeS absorbers, which, to date, have been rarely obtained from conventional CZTS-derivative nanoparticles with organic capping molecules.

To confirm the compositional grading in the annealed absorber films, we utilized secondary ion mass spectrometry (SIMS) (Figure 4a). It was observed that the Sn/(Ge+Sn) ratio decreased monotonically toward the bottom layer, while the compositions of Cu, Zn, and S remained constant across the depth. The detected carbon concentration was nearly negligible in the overall film, confirming the formation of a carbon-free absorber layer. To investigate how the bandgap was graded in connection with the compositional distribution, we calculated the bandgap energy distribution along the film thickness, based on the compositional dependence of the bandgap energy obtained in Figure S2 (Supporting Information), and the SIMS composition profile (Figure 4b).[28] In the SIMS analysis, the sputtering rate was ~0.6 nm/s. Using this etching rate, we converted the sputtering time to a detection position. The Cu, Zn, Ge, and Sn components were undetectable below the calculated thickness of 1.1 μm, which matched reasonably well with the thickness observed in the FE-SEM images. Interestingly, the resulting absorber layer exhibited a gradual grading in band structure, even though the film was made using three different NCs with different $Sn_2S_6^{4-}$ ligand concentrations; this implies the Sn atoms are capable of diffusing spatially when thermal energy is supplied during annealing. To further measure the energy states in conjunction with the calculated bandgap distribution, we performed inverse photoelectron spectroscopy (IPES) and ultraviolet photoelectron spectroscopy (UPS) analyses. From these, the valence band maximum (VBM) and the conduction band minimum (CBM) levels across the depth of the film were determined by measurement combined with Ar ion beam etching (Supporting Information, Figure S5). The intersections in UPS and IPES edges with respect to the background, obtained by a linear extrapolation (red solid lines), determine the VBM and the CBM, respectively.[28,29] The VBM was almost similar, regardless of the positions, whereas the CBM varied depending on the etching time. It has been reported that the VBM mainly depends on the Cu composition in CZTGeS films, because the Cu *d* and anion *p* orbital hybridization alters the valence energy state.[25] Similar VBM values were obtained across the depth, which is attributable to the invariance of Cu composition in the CZGTeS films, as confirmed by SIMS analysis. By contrast, CBM values depend on the Sn/(Ge+Sn) ratio; thus, in our study, CBM decreased gradually from the back contact toward

dx.doi.org/10.1021/cm501568d | *Chem. Mater.* 2014, 26, 3957−3965

the $p-n$ junction, showing the band grading structure produced by the change of the CBM level. The upshifted CBM reduces the band offset between the CdS and CZTGeS layer. The CBM of the CdS layer is higher than that of the CZTS layer, so it creates a band offset barrier at an interface (~0.2 eV). In Ge-doped CZTS layers, the CBM moves up depending on the Ge doping concentration, relieving the offset and, in turn, reducing the recombination probability. An excessive Ge concentration, which moves the CBM above the level for ~1.7 eV in a bandgap, instead degrades the open-circuit voltage.[30] This is the reason we chose the value of ~1.65 eV as the bandgap of the top surface in the CZTGeS absorber layers, using CZTGeS NCs exchanged in a 2.5 M ligand solution. The UPS and IPES analyses allowed us to depict the band diagram for our graded CZTGeS film, as shown in Figure 4c. The sputtering rate was ~1 nm/s in both analyses. Compared with the bandgap profile predicted from the SIMS result, in which the bang gap varied from 1.65 to 1.84 eV, a very similar band grading structure was suggested by the UPS/IPES analyses. The CZTGeS layer at the $p-n$ junction had the bandgap of 1.62 eV, which increased, reaching 1.85 eV, at the back contact. This observation clearly supports the conclusion that a bandgap-graded absorber can be achieved from NCs capped by MCC ligands with different compositions. Using this bandgap-graded absorber layer, we fabricated thin-film solar cells in a standard configuration, by the successive deposition of CdS, intrinsic zinc oxide (i-ZnO), and indium tin oxide (ITO), as shown in Figure 4d.

Figure 5a shows the current–voltage ($J-V$) characteristics of the CZTGeS thin-film solar cells. Among the various $J-V$ data, we tried to compare the cell performance using the best efficiency. First, we compared the OLA capped and MCC capped NCs derived ungraded cells. Both ungraded cells had the same Ge/Sn ratio, allowing us to investigate the influence of different ligand types. The best performing MCC capped NCs-based CZTGeS device exhibited an efficiency of 4.8% [V_{OC} = 0.50 V, J_{SC} = 19.72 mA cm^{-2}, FF = 49.5%], whereas the best performing OLA capped NCs-based cell had an efficiency of 3.6% [V_{OC} = 0.49 V, J_{SC} = 17.16 mA cm^{-2}, FF = 43.3%] (Supporting Information, Figure S6). The improved cell performance of the MCC capped ungraded cell was characterized by larger J_{SC} and FF values. As described above, the OLA capping ligands with long chains were not completely decomposed even after high temperature sulfurization, leaving behind carbonaceous impurities at the bottom of the absorber layer. It is thought that this impurity phase likely increases the series resistance of the cell, which interrupts the carrier collection at the back contact and, in turn, decreases the J_{SC} and FF values. Second, we compared the performance of the MCC capped NCs derived bandgap-graded CZTGeS cell with the MCC capped NCs derived ungraded bandgap cell. The best performing bandgap-graded CZTGeS device showed a significantly improved efficiency of 6.3% [V_{OC} = 0.54 V, J_{SC} = 23.36 mA cm^{-2}, FF = 50.0%]. To show the reproducibility of our solar cells, the performance statistics based on 15 devices are shown in Table 2 and Figures S7–9 (Supporting Information). Compared with the device parameters of the ungraded solar cell, both the short-circuit current density and open-circuit voltage of the bandgap-graded cell were considerably increased, resulting in the improvement of cell efficiency. For the ungraded solar cell, the carriers generated deep inside the absorber layer do not experience sufficient driving force to move them toward a junction for charge collection. In contrast, in the bandgap-graded cell, the additional electric field arising

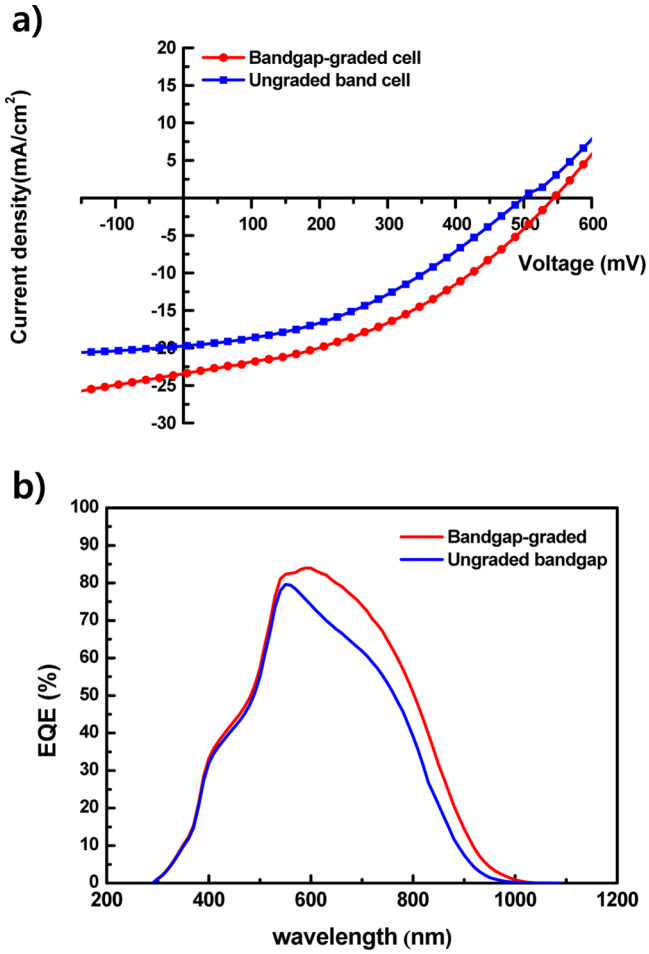

Figure 5. (a) $J-V$ characteristics for the bandgap-graded CZTGeS thin-film solar cells compared to ungraded bandgap structured device (annealed under Ar+H_2S (4%) at 530 °C, 30 min). All device performance parameters are based on the effective area (0.21 cm^2), excluding the area shaded by the Ni/Al finger electrode. (b) EQE curve of the bandgap-graded CZTGeS thin-film solar cell compared with the ungraded bandgap device.

from the potential difference in conduction band helps carriers to drift toward the space-charge depletion region and consequently the carrier collection can be enhanced. External quantum efficiency (EQE) analysis was performed for both graded and ungraded cells to confirm the effect of bandgap grading on carrier collection, as shown in Figure 5b. In the wavelength range from 300 to 550 nm, there was no significant difference. However, at longer wavelengths (550 nm < λ < 1000 nm), the bandgap-graded cell exhibited a higher spectral response than the ungraded device. This result indicates that the carriers generated at the bottom of the CZTGeS layer move toward the junction more effectively in the case of a bandgap-graded cell, contributing to the enhancement of carrier collection. Therefore, it is thought that this enhanced carrier collection produced by the bandgap grading is responsible for the higher short circuit current in the bandgap-graded CZTGeS cell. In addition, bandgap grading can also increase the open-circuit voltage due to the lower recombination rate at a higher band gap location.[14,32] This is why the V_{OC} value of the graded solar cell is larger than that of the ungraded cell. The FF, series resistance, and shunt resistance for both cells showed similar values (Table 2). It can be expected that both cells, having

dx.doi.org/10.1021/cm501568d | Chem. Mater. 2014, 26, 3957–3965

Table 2. Device Characteristics of the OLA Capped CZTGeS and the MCC Ligand-Exchanged NCs-based CZTGeS Solar Cells[a]

cell	PCE [%]	FF [%]	V_{OC} [V]	J_{SC} [mA/cm^2]	R_s[b] [Ωcm^2]	R_{sh}[c] [Ωcm^2]
OLA capped ungraded bandgap	3.4(±0.25)	39.4(±2.0)	0.48(±0.01)	17.13(±0.1)	6.5(±0.2)	1348.7(±17)
MCC capped ungraded bandgap	4.6(±0.20)	48.7(±3.0)	0.48(±0.02)	19.55(±0.2)	4.2(±0.3)	1318.5(±15)
MCC capped bandgap-graded	6.0(±0.30)	49.6(±3.5)	0.52(±0.01)	23.28(±0.2)	4.1(±0.2)	1335.2(±20)

[a]The depth compositions of the absorber layers were either homogeneous or graded. The films were annealed at 530 °C for 30 min on Mo substrate under Ar+H_2S (4%) atmosphere. The data shown are the average value and standard deviation obtained from 15 devices. [b]Series resistance (R_s) is determined based on voltage difference at the maximum power points between the one-sun $J-V$ curve and the dark $J-V$ curve, which is shifted by the short circuit current density J_{sc}, as proposed by Aberle.[31] [c]Shunt resistance (R_{sh}) is the change in the voltage for change in the current density at 0 V on the dark $J_{sc}-V_{oc}$ curve.

similar cell thickness, were fabricated by identical annealing conditions, thereby resulting in the similar interface quality. To elucidate the stability of our cells, we kept the 15 cells of each type for 30 days under ambient conditions and measured the performance. As shown in Table S3 (Supporting Information), the decrease of 0.4−0.5% in conversion efficiencies was observed for all the aged cells. It is presumed that this slight degradation might be caused by either the surface oxidation or the adverse effect by moistures; however, the cell performance approaching 90% of as-fabricated fresh cells was maintained even after 1 month. It is highly expected that the device stability can be further improved with a proper passivation.

CONCLUSIONS

We demonstrated the synthesis of bandgap tunable CZGeS NCs capped with $Sn_2S_6^{4-}$ MCC ligands. Ligand exchange was performed at different concentrations of $(NH_4)_4Sn_2S_6$ solution, which allowed the removal of the OLA organic ligand and produced CZGeS NCs with varying absorbed amounts of $Sn_2S_6^{4-}$. A carbon free bandgap-graded CZTGeS absorber was fabricated by successive coatings of CZGeS NCs inks with three different MCC ligand compositions. Elemental analysis and spectroscopic measurement confirmed that the Sn/(Ge+Sn) ratio varied across the depth of the annealed absorbers, which resulted in the variation of the bandgap from 1.62 eV, at a back contact, to 1.85 eV, at the $p-n$ junction. We successfully demonstrated a PCE of 6.3% for the bandgap-graded device, while an efficiency of 4.8% was achieved for the ungraded cell. Our findings provide a simple and facile approach to tune the bandgap of the absorber layer using MCC capped NCs with different surface Sn contents, which enabled us to fabricate high-efficiency solar cells without an additional selenization process.

ASSOCIATED CONTENT

Supporting Information

ICP-AES and TG-DSC analyses of OLA- CZTGeS NCs and $Sn_2S_6^{4-}$ MCC capped CZGeS NCs, FESEM image of the as-prepared and the annealed CZTGeS films, cross sectional EDX line scan data to confirm the composition of bottom layer, plot of the optical bandgap of the annealed CZTGeS films measured by UV−vis spectra vs Sn/(Ge+Sn) ratio, the results of UPS and IPES analyses, statistics data of each cell (V_{OC}, J_{SC}, FF and PCE), $J-V$ curve data of OLA capped CZTGeS cell, stability data of each cell. This material is available free of charge via the Internet at http://pubs.acs.org.

AUTHOR INFORMATION

Corresponding Authors

*J. Moon. E-mail: jmoon@yonsei.ac.kr. Tel.: +82-2-2123-2855. Fax: +82-2-312-5375.

*S. Jeong. E-mail: sjeong@krict.re.kr. Tel.: +82-42-860-7368. Fax: +82-42-861-7022.

Notes

The authors declare no competing financial interest.

ACKNOWLEDGMENTS

This research received financial support from a National Research Foundation of Korea (NRF) grant funded by the Korea government (MSIP) (No. 2012R1A3A2026417). It was also partially supported by the third Stage of Brain Korea 21 Plus Project.

REFERENCES

(1) Todorov, T. K.; Gunawan, O.; Gokmen, T.; Mitzi, D. B. *Prog. Photovoltaics: Res. Appl.* **2013**, *21*, 82−87.
(2) Todorov, T. K.; Mitzi, D. B. *Eur. J. Inorg. Chem.* **2010**, *1*, 17−28.
(3) Ki, W.; Hillhouse, H. W. *Adv. Energy Mater.* **2011**, *1*, 732.
(4) Riha, S. C.; Parkinson, B. A.; Prieto, A. L. *J. Am. Chem. Soc.* **2009**, *131*, 12054−12055.
(5) Zhou, H.; Hsu, W.-C; Duan, H.-S; Bob, B.; Yang, W.; Song, T.-B.; Hsu, C.-J.; Yang, Y. *Energy Environ. Sci.* **2013**, *6*, 2822−2838.
(6) Miskin, C. K.; Yang, W.-C.; Hages, C. J.; Carter, N. J.; Joglekar, C. S.; Stach, E. A.; Agrawal, R. *Prog. Photovoltaics: Res. Appl.* **2014**, DOI: 10.1002/pip.
(7) Cao, Y.; Denny, M. S., Jr.; Caspar, J. V.; Farneth, W. E.; Guo, Q.; Ionkin, A. S.; Johnson, L. K.; Lu, M.; Malajovich, I.; Radu, D.; Rosenfeld, H. D.; Choudhury, K. R.; Wu, W. *J. Am. Chem. Soc.* **2012**, *134*, 15644−15647.
(8) Robel, I.; Subramanian, V.; Kuno, M.; Kamat, P. V. *J. Am. Chem. Soc.* **2006**, *128*, 2385−2393.
(9) Rogach, A. L.; Franzl, T. T.; Klar, A.; Feldmann, J.; Gaponik, N.; Lesnyak, V.; Shavel, A.; Eychmüller, A.; Rakovich, Y. P.; Donegan, J. F. *J. Phys. Chem. C* **2007**, *111*, 14628−14637.
(10) Guo, Q.; Ford, G. M.; Hillhouse, H. W.; Agrawal, R. *Nano Lett.* **2009**, *9*, 3060−3065.
(11) Panthani, M. G.; Akhavan, V.; Goodfellow, B.; Schmidtke, J. P.; Dunn, L.; Dodabalapur, A.; Barbara, P. F.; Korgel, B. A. *J. Am. Chem. Soc.* **2008**, *130*, 16770−16777.
(12) Kim, Y.; Woo, K.; Kim, I.; Cho, Y. S.; Jeong, S.; Moon, J. *Nanoscale* **2013**, *5*, 10183.
(13) Hages, C. J.; Levcenco, S.; Miskin, C. K.; Alsmeier, J. H.; Abou-Ras, D.; Wilks, R. G.; Bär, M.; Unold, T.; Agrawal, R. *Prog. Photovoltaics: Res. Appl.* **2013**, DOI: 10.1002/pip.2442.
(14) Lundberg, O.; Edoff, M.; Stolt, L. *Thin Solid Films* **2005**, *480−481*, 520−525.
(15) Ford, G. M.; Guo, Q.; Agrawal, R.; Hillhouse, H. W. *Chem. Mater.* **2011**, *23*, 2626−2629.
(16) Akhavan, V. A.; Goodfellow, B. W.; Panthani, M. G.; Steinhagen, C.; Harvey, T. B.; Stolle, C. J.; Korgel, B. A. *J. Solid State Chem.* **2012**, *189*, 2−12.
(17) Lee, E.; Park, S. J.; Cho, J. W.; Gwak, J.; Oh, M.-K.; Min, B. K. *Sol. Energy Mater. Sol. Cells* **2011**, *95*, 2928−2932.
(18) Kovalenko, M. V.; Scheele, M.; Talapin, D. V. *Science* **2009**, *324*, 1417−1420.

(19) Kovalenko, M. V.; Bodnarchuk, M. I.; Zaumseil, J.; Lee, J.-S.; Talapin, D. V. *J. Am. Chem. Soc.* **2010**, *132*, 10085−10092.
(20) Nag, A.; Kovalenko, M. V.; Lee, J.-S.; Liu, W.; Spokoyny, B.; Talapin, D. V. *J. Am. Chem. Soc.* **2011**, *133*, 10612−10620.
(21) Stolle, C. J.; Panthani, M. G.; Harvey, T. B.; Akhavan, V. A.; Korgel, B. A. *ACS Appl. Mater. Interfaces.* **2012**, *4*, 2757−2761.
(22) Contreras, M. A.; Tuttle, J.; Gabor, A.; Tennant, A.; Ramanathan, K.; Asher, S.; Franz, A.; Keane, J.; Wang, L.; Scofield, J.; Noufi, R. *Sol. Energy Mater. Sol. Cells* **1996**, *41/42*, 231−246.
(23) Chen, S.; Yang, J.-H.; Gong, X. G.; Walsh, A.; Wei, S.-H. *Phys. Rev. B* **2010**, *81*, 245204.
(24) Guc, M.; Izquierdo-Roca, V.; Rodiguez, A. P.; Gurieva, G.; Levcenko, S.; Schorr, S.; Arushanov, E. *Phys. Status Solidi C* **2013**, *10*, 1075−1081.
(25) Guo, Q.; Ford, G. M.; Yang, W.-C.; Hages, C. J.; Hillhouse, H. W. *Sol. Energy Mater. Sol. Cells* **2012**, *105*, 132−136.
(26) Dullweber, T.; Hanna, G.; Shams-Kolahi, W.; Schwartzlander, A.; Contreras, M. A.; Noufi, G. R.; Schock, H. W. *Thin Solid Films* **2000**, *361−362*, 478−481.
(27) Chirila, A.; Buecheler, S.; Pianezzi, F.; Bloesch, P.; Gretener, C.; Uhl, A. R.; Fella, C.; Kranz, L.; Perrenoud, J.; Seyrling, S.; Verma, R.; Nishiwaki, S.; Romanyuk, Y. E.; Bilger, G.; Tiwari, A. N. *Nat. Mater.* **2011**, *10*, 857−861.
(28) Bar, M.; Schubert, B. A.; Marsen, B.; Wilks, R. G.; Pookpanratana, S.; Blum, M.; Krause, S.; Unold, T.; yang, W.; Weinhardt, L.; Heske, C.; Schock, H. W. *Appl. Phys. Lett.* **2011**, *99*, 222105.
(29) Yun, D.-J.; Chung, J.; Jung, C.; Han, H.-S.; Lee, J.; Anass, B.; Lee, S.; Kyung, Y.; Park, S.-H. *J. Electrochem. Soc.* **2013**, *160*, H436−H442.
(30) Nagoya, A.; Asahi, R.; Kresse, G. *J. Phys.: Condens. Matter* **2011**, *23*, 404203.
(31) Aberle, A. G.; Wenham, S. R.; Green, M. A. *Proceedings of the 23rd IEEE Photovoltaic Specialists Conference*, Louisville, KY, May, 1993; IEEE: New York, 1993; pp 133−139.
(32) Dullweber, T.; Hanna, G.; Rau, U.; Schock, H.-W. *Sol. Energy Mater. Sol. Cells* **2001**, *67*, 145−150.